

Journal of Biomedical Optics

SPIEDigitalLibrary.org/jbo

Investigation of the cerebral hemodynamic response function in single blood vessels by functional photoacoustic microscopy

Lun-De Liao
Chin-Teng Lin
Yen-Yu I. Shih
Hsin-Yi Lai
Wan-Ting Zhao
Timothy Q. Duong
Jyh-Yeong Chang
You-Yin Chen
Meng-Lin Li

Investigation of the cerebral hemodynamic response function in single blood vessels by functional photoacoustic microscopy

Lun-De Liao,^{a,b} Chin-Teng Lin,^{a,b} Yen-Yu I. Shih,^c Hsin-Yi Lai,^a Wan-Ting Zhao,^d Timothy Q. Duong,^c Jyh-Yeong Chang,^a You-Yin Chen,^{a,e} and Meng-Lin Li^f

^aNational Chiao Tung University, Department of Electrical Engineering, Hsinchu, Taiwan

^bNational Chiao Tung University, Brain Research Center, Hsinchu, Taiwan

^cUniversity of Texas Health Science Center at San Antonio, Research Imaging Institute, San Antonio, Texas

^dNational Taiwan University, Institute of Zoology, Taipei, Taiwan

^eNational Yang Ming University, Department of Biomedical Engineering, Taipei, Taiwan

^fNational Tsing Hua University, Department of Electrical Engineering, Hsinchu, Taiwan

Abstract. The specificity of the hemodynamic response function (HRF) is determined spatially by the vascular architecture and temporally by the evolution of hemodynamic changes. Here, we used functional photoacoustic microscopy (fPAM) to investigate single cerebral blood vessels of rats after left forepaw stimulation. In this system, we analyzed the spatiotemporal evolution of the HRFs of the total hemoglobin concentration (HbT), cerebral blood volume (CBV), and hemoglobin oxygen saturation (SO₂). Changes in specific cerebral vessels corresponding to various electrical stimulation intensities and durations were bilaterally imaged with 36 × 65-μm² spatial resolution. Stimulation intensities of 1, 2, 6, and 10 mA were applied for periods of 5 or 15 s. Our results show that the relative functional changes in HbT, CBV, and SO₂ are highly dependent not only on the intensity of the stimulation, but also on its duration. Additionally, the duration of the stimulation has a strong influence on the spatiotemporal characteristics of the HRF as shorter stimuli elicit responses only in the local vasculature (smaller arterioles), whereas longer stimuli lead to greater vascular supply and drainage. This study suggests that the current fPAM system is reliable for studying relative cerebral hemodynamic changes, as well as for offering new insights into the dynamics of functional cerebral hemodynamic changes in small animals. © 2012 Society of Photo-Optical Instrumentation Engineers (SPIE). [DOI: 10.1117/1.JBO.17.6.061210]

Keywords: functional photoacoustic microscopy; electrical stimulation; total hemoglobin concentration; hemoglobin oxygen saturation.

Paper 11507SS received Sep. 14, 2011; revised manuscript received Dec. 22, 2011; accepted for publication Jan. 16, 2012; published online May 7, 2012.

1 Introduction

To understand the hemodynamic response function (HRF) in single cerebral blood vessels, it is crucial to image changes in total hemoglobin concentration (HbT), cerebral blood volume (CBV), and hemoglobin oxygen saturation (SO₂).^{1,2} The most prominent neuroimaging technique, functional magnetic resonance imaging (fMRI), maps brain function by measuring surrogate changes in cerebral blood flow (CBF), CBV, and oxygenation that accompany changes in neural activity. Although, a remarkable association exists between changes in neural activity and the hemodynamic state, a complete understanding of the spatiotemporal evolution of the cerebral HRF is still missing. Recently, Hirano et al. investigated changes in CBF and CBV during forelimb stimulations of various durations in an anesthetized rodent model.³ However, fMRI measures only changes in selected pixels located in the activation region in response to a stimulus. It is still difficult to image HRF changes in single cerebral blood vessels using fMRI without the use of contrast agents.⁴ Recently, optical brain imaging has been increasingly used to study brain functions *in vivo*⁵

because it can measure oxy-hemoglobin (HbO₂) and deoxy-hemoglobin (Hb) through the models' distinctive optical absorption characteristics.⁵⁻⁸ Diffusion optical imaging (DOI)^{9,10} and laser speckle imaging (LSI)^{11,12} are the two most widely used optical imaging techniques for the *in vivo* imaging of cerebral hemodynamic changes. The DOI technique can acquire CBV, HbO₂ and Hb signals directly through the intact skull and track their changes noninvasively in response to an electrical stimulation of the rat forepaw.⁹ Recently, Sigel et al. performed a temporal comparison of the functional changes in HbO₂ and Hb by DOI and fMRI during different durations of stimulation of the rat forepaw. Their results suggest that the HRF changes measured by DOI and fMRI are qualitatively similar, and that the use of optical imaging techniques to investigate changes in neurovascular coupling is becoming increasingly reliable in small animal models. However, for DOI, SO₂ quantification is problematic due to tissue scattering and the nonlinear relationship between signal intensity and absorption coefficients.^{8,13,14} This problem also impairs the visualization of HRF changes in single blood vessels. In contrast, LSI can probe the hemodynamic changes in single blood vessels with high spatial resolution after the skull has been removed.¹⁵ Bouchard et al. proposed a novel system that, at a lower cost, enables simultaneous

Address all correspondence to: You-Yin Chen, National Yang Ming University, Department of Biomedical Engineering, Taipei, Taiwan; E-mail: irradiance@so-net.net.tw, Meng-Lin Li, National Tsing Hua University, Department of Electrical Engineering, Hsinchu, Taiwan. Tel: +886 3 516 2179; Fax: +886 3 571 5971; E-mail: mlli@ee.nthu.edu.tw

visualization of HbT, HbO₂, and Hb dynamics within single blood vessels during forepaw stimulation.¹⁵ However, due to the limited penetration depth and poor depth resolution of LSI, it can access information only from single blood vessels that reflect from the cortical surface.^{11,12,16}

Functional photoacoustic microscopy (fPAM), which can measure functional hemoglobin changes in single blood vessels without a labeling agent, is ideal for the *in vivo* imaging of changes in HbT, CBV, and SO₂. Recently, photoacoustic (PA) imaging has been applied to subcutaneous vasculature imaging,¹⁷ breast tumor detection,¹⁸ and oxygenation monitoring in blood vessels.^{19,20} Our recent study utilized the fPAM capability of acquiring relative functional hemodynamic responses to forepaw electrical stimulation in exposed rodent brains.²¹ Our findings indicate that hemodynamic changes in specific cortical regions of the brain can be reliably imaged using fPAM.

In this study, the fPAM system was used to investigate functional HRF changes in HbT, CBV, and SO₂ within specific cerebral blood vessels. Bilateral neurovascular changes were elicited by left forepaw electrical stimulation with various stimulation parameters. We studied the temporal dependence of the changes in specific cerebral vessels, using different stimulation intensities and durations and performed comprehensive characterization of vascular dynamics. This technique has the potential to advance our understanding of changes in cerebral neurovascular coupling and to improve the monitoring of cerebral HRF changes in small animal models.

2 Materials and Methods

2.1 Dark-Field Confocal fPAM System

A 50-MHz dark-field confocal fPAM system was used to image the functional changes in specific cortical vessels. Laser pulses were generated by an optical parametric oscillator (Surlite OPO Plus, Continuum, Santa Clara, CA) pumped by a frequency-tripled Nd:YAG Q-switched laser (Surlite II-10, Continuum), which provides ~4-ns laser pulses at a pulse repetition rate of 10 Hz. Laser pulses at two visible wavelengths, 560 (λ_{560}) and 570 nm (λ_{570}), were used for PA wave excitation. To probe the relative changes in HbT, CBV, and SO₂ in specific blood vessels, these two wavelengths have been optimized to provide high signal-to-noise ratios (SNRs) and sensitivity.²¹ The 50-MHz ultrasonic transducer used in the current fPAM system was custom-made by the Resource Center for Medical Ultrasonic Transducer Technology at the University of Southern California (<http://bme.usc.edu/UTRC/>). It has a 6-dB fractional bandwidth of 57.5%, a focal length of 9 mm, and a 6-mm active element, offering an axial resolution of 36 μ m and a lateral resolution of 65 μ m.

Laser energy was delivered by a 1-mm multimode fiber. The fiber tip was coaxially aligned with a convex lens, an axicon, a plexiglass mirror, and an ultrasonic transducer on an optical bench, forming dark-field illumination that is confocal with the focal point of the ultrasonic transducer. The incident energy density on the sample surface was well within the safety limit of the American National Standards Institute (ANSI). During the imaging process, the transducer was immersed in an acrylic water tank with a hole in the bottom that was sealed with a piece of 15- μ m-thick polyethylene film. A thin layer of ultrasonic gel was applied onto the rat's head and then attached to the thin film in order to ensure good coupling of PA waves to the tank. The PA signals received by the ultrasonic transducer were

preamplified by a low-noise amplifier (noise figure 1.2 dB, gain 55 dB, AU-3A-0110, Miteq, Hauppauge, NY) and cascaded to an ultrasonic receiver (5073 PR, Olympus, Center Valley, PA). Then, the signals were digitized and sampled by a computer-based, 14-bit analog-to-digital (A/D) card (CompuScope 14200, GaGe, Lockport, IL) at a 200-MHz sampling rate for data storage. The fluctuations in the laser energy were monitored by a photodiode (DET36A/M, Thorlabs, Newton, NJ). Finally, the recorded photodiode signals were applied to compensate for PA signal variations caused by laser energy instability before any further signal processing.

The achievable penetration depth of the fPAM is 3 mm, and the SNR (defined as the ratio of the signal peak value to the rms value of the noise) is ~18 dB. Three scanning types can be provided by this system to image the region of interest: A-line (one-dimensional images where the axis represents the imaging depth), B-scan (two-dimensional images where one axis is the lateral scanning distance and the other is the imaging depth), and C-scan (projection images from the three-dimensional images). To speed up the imaging of the rapid hemodynamic response in the subsequent functional imaging analysis, no signal averaging in time was performed. Note that the amplitude of the envelope-detected PA signal was used in the functional imaging analysis.

2.2 Experimental Animals

Six male Wistar rats (National Laboratory Animal Center, Taiwan), weighing 250 to 300 g each, were used. The animals were housed at a constant temperature and humidity with free access to food and water. Before the imaging experiments, the rats fasted for 24 h but were given water *ad libitum*. All animal experiments were conducted in accordance with the guidelines of the Animal Research Committee of National Chiao Tung University and National Tsing Hua University. The animals were initially anesthetized with 3% isoflurane. Supplemental α -chloralose anesthesia (70 mg/kg) was injected intraperitoneally as needed. The anesthetized rats were mounted on a custom-made acrylic stereotaxic head holder to reduce motion artifacts during the experiment, and the skin and muscle were cut away from the skull to expose the bregma landmark. The anteroposterior (AP) distance between the bregma and the interaural line²² was surveyed directly. The bregma was 9.3 ± 0.12 mm [mean \pm standard deviation (SD)] anterior to the interaural line.²³ Next, a craniotomy was performed on each animal, and a bilateral cranial window of approximately 8 (horizontal) \times 6 (vertical) mm² was made with a high-speed drill. After the rat was secured to the stereotaxic frame and placed on the bed pallet, the pallet was moved into position at the bregma, which was 9 mm anterior to an imaginary line drawn between the center of each ear bar (the interaural line).²¹ In the subsequent experiments, the interaural and bregma references were then used to position the head in the fPAM system without additional surgery.

After bregma positioning, a PA C-scan (i.e., a projection image from the three-dimensional images) was performed to acquire reference images of the cortical vasculature. The cortical blood vessels under the open-skull window of the rat cortical surface, indicated by solid red arrows in Fig. 1(a), were imaged *in vivo* by fPAM at λ_{570} , as shown in Fig. 1(b). In addition, arteriolar branches from the anterior cerebral artery (ACA) vessel system can be seen in the projected C-scan image.^{24,25} These were bilaterally identified as MI and MII and are labeled in

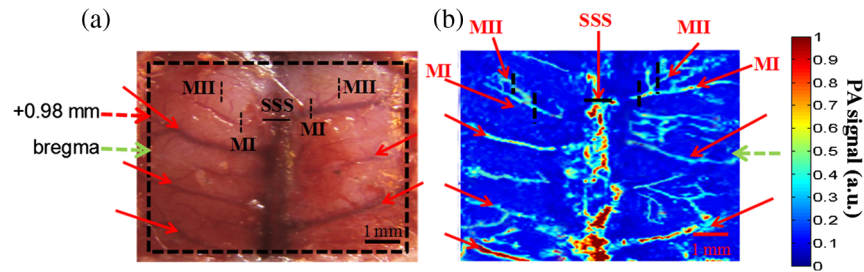


Fig. 1 Comparison of an open-skull photograph with a PA-projected C-scan image acquired at λ_{570} . (a) An open-skull photograph of the cerebral surface showing an unobstructed view of the cortex vessels. Some branches of the blood vessels, which are indicated by the red solid arrows, are imaged by fPAM in (b). The green dashed line indicates the position of the bregma. The red dashed arrow indicates the section of the bregma +0.98 mm activated during left forelimb stimulation. (b) *In vivo* PA-projected C-scan image of the blood vessels in the superficial layer of the cortex acquired at λ_{570} . The green dashed arrow indicates the position of the bregma. The SSS and some cortical vessels on the cortical surface can be identified. Functional B-scan images of the SSS and bilateral MI and MII arterioles were acquired by scanning along the black solid and dashed lines in the bilateral region.

both Fig. 1(a) and 1(b), along with the superior sagittal sinus (SSS). The SSS is the largest vein in the rodent brain cortex.²⁵ The MI and MII arterioles are two different-sized arterioles that branch from the ACA blood vessel system and extend from the bottom center of the brain to the cortical surface. The bilateral MI arterioles cross through the anatomical borders of the primary motor cortex and secondary motor cortex.²⁵ However, the bilateral MII arterioles are located in the anatomical borders of the primary somatosensory cortex that innervates the forepaw (S1FL).^{25,26} Functional changes in HbT, CBV, and SO_2 in the SSS and the bilateral MI and MII arterioles were imaged by fPAM scanning during stimulation. These images were acquired along the black solid and dashed lines in the bilateral regions shown in Fig. 1(b). Moreover, some branches of these vessels were also visualized in the projected C-scan image. Note that the SSS was not imaged well by the current fPAM system, which is similar to previous reports.^{21,27} The geometric focusing and the finite detection bandwidth of the ultrasound transducer that was used may have accounted for the weakness of the PA signals detected from the SSS.²⁸ Sensing with spherical geometric focusing inherently preferred point-like PA sources, which was not applicable to the PA signals of the SSS because of its large size. In addition, the frequency of the PA signal generated by the SSS might be out of the detection bandwidth of the transducer, thus weakening the detected PA signals.

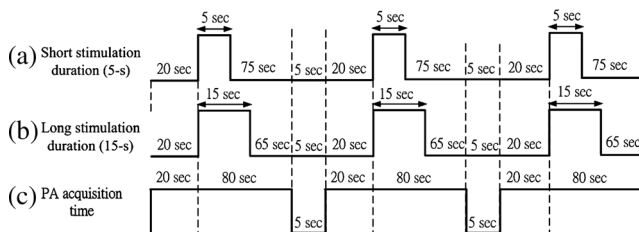


Fig. 2 Schematic diagram of the experimental protocol, including the two different stimulations and the fPAM imaging timing. (a) Block design utilized for the short electrical forepaw stimulation task (5 s). (b) Block design utilized for the long electrical forepaw stimulation task (15 s). (c) PA data were acquired in three active blocks under different stimulation intensities. Multiple PA B-scan images of specific single cortical vessels were acquired in each active block. Note that in (b) and (c), the task began at the baseline “Stimulation-OFF” state; the active “Stimulation-ON” state consisted of a constant 0.2-ms electrical pulse width, a 3-Hz pulse train and a pulse amplitude of 1, 2, 6, or 10 mA. There was a 5-s lapse between the PA scan and the block-design paradigm to the next block.

2.3 Electrical Forepaw Stimulation

Forepaw stimulation was applied to evoke functional hemodynamic changes in the cerebral vessels, and it was achieved by insertion of thin-needle stainless electrodes under the skin of the rat’s left forepaw. Electrical stimulation was then applied using a stimulator (Model 2100, A-M Systems, Sequim, WA). A monophasic constant current of four pulses of different intensities (1, 2, 6, and 10 mA) with a 0.2-ms pulse width at a frequency of 3 Hz was used. Various stimulation intensities were employed to evoke hemodynamic changes of different strengths during the stimulation onset. In addition, two stimulation durations of 5 and 15 s were employed. A block-design paradigm was employed in this study for functional signal acquisition. The short stimulation duration (5 s) was originally selected to provide enough time for the hemodynamic response to reach a maximum value in order to enable the large amount of averaging necessary.²⁹ The longer stimulation duration (15 s) was selected to enable the cerebral volume response to reach a nearly maximal response while avoiding the progressive attenuation that is seen for stimuli of longer durations.³⁰ Each trial consisted of three blocks, and each block began with a 20-s baseline that was followed by a 5-s Stimulation-ON and a 75-s Stimulation-OFF period for the shorter stimulation or a 15-s Stimulation-ON and a 65-s Stimulation-OFF period for the longer stimulations, as illustrated in Fig. 2(a) and 2(b). There was a 5-s lapse between each block, and the PA signals [Fig. 2(c)] at λ_{560} or λ_{570} were acquired in each block to assess stimulation-induced hemodynamic changes in specific single cortical vessels (the SSS and bilateral MI and MII arterioles). Note that the timing used in our block-design paradigm is adequate for the rat’s brain to recover to the resting state before the next stimulus.³¹

2.4 Data Analysis of the Functional Changes in CBV, HbT, and SO_2

Two optimized wavelengths (i.e., λ_{560} and λ_{570}) were employed to monitor functional HbT, CBV, and SO_2 changes with a high SNR and high sensitivity.²¹ It was assumed that the CBV is proportional to the cross-sectional area of a single blood vessel.³² Functional CBV changes (R_{CBV}) in a single vessel can be monitored by assessing the changes in the cross-section of the vessel during each block against a cross-section baseline acquired immediately before the electrical stimulation onset (i.e., ~ 20 s in each block). PA cross-sectional B-scan images of

each specific single vessel at λ_{570} [i.e., $I_{R(570)}$] were used. $R_{CBV}(t)$ was constructed according to the following equation:

$$R_{CBV}(t) = \frac{A[I_{R(570)}(t)]}{A[I_{R(570),baseline}]}, \quad (1)$$

where t is the time in each block, $A[I_{R(570)}(t)]$ represents the cross-sectional area of a single vessel at a given time in each block, and $A[I_{R(570),baseline}]$ is the cross-section baseline estimated from the baseline image acquired immediately before electrical stimulation onset in each block. $A[I_{R(570)}]$ was calculated from the total vessel pixel count of a single vessel image [i.e., $I_{R(570)}$]. A vessel pixel was defined as any pixel with a PA signal three times greater than the background signal.^{21,33}

The optical absorption of blood at λ_{570} is insensitive to the SO_2 level because λ_{570} is an isosbestic point of the molar extinction spectra of HbO_2 and Hb. That is, changes in the PA signal at λ_{570} largely result from changes in the total amount of hemoglobin (i.e., HbT) within the PA resolution cell ($HbT = [HbO_2] + [Hb]$).²⁷ Therefore, PA B-scan images at λ_{570} [$I_{R(570)}$] were used to probe the changes in HbT. Because the PA signal at a given pixel in $I_{R(570)}$ is proportional to the HbT within the PA resolution cell centered at that pixel, the mean functional HbT changes [$R_{HbT}(t)$] in a single vessel during the stimulation period could be assessed as follows:

$$R_{HbT}(t) = \frac{\sum_{(x,y) \in \text{vessel pixel}} [I_{R(570)}(x, z, t)]/A[I_{R(570)}(t)]}{\sum_{(x,y) \in \text{vessel pixel}} [I_{R(570),baseline}(x, z, t)]/A[I_{R(570),baseline}(t)]}, \quad (2)$$

where (x, z) is the pixel position and $I_{R(570),baseline}$ is the baseline image at λ_{570} acquired immediately before electrical stimulation onset in each block.

In contrast to those at λ_{570} , PA signal changes at λ_{560} were sensitive to SO_2 changes because the largest absorption changes in the visible spectrum occur at approximately λ_{560} , when the SO_2 level changes. To exclude the effects of changes in HbT on PA signals and to observe only the SO_2 level changes,²¹ functional images of SO_2 changes [$\Delta I_{F(560)}(t)$] at the given time point t in each block were then assessed according to the following equation:

$$\begin{aligned} \Delta I_{F(560)}(t) &= \frac{I_{F(560)}(t)}{I_{R(570)}(t)} - \frac{I_{F(560),baseline}}{I_{R(570),baseline}} \\ &= I_{F(560)}(t) - I_{F(560),baseline}, \end{aligned} \quad (3)$$

where $I_{F(560)}$ (i.e., the PA image acquired at λ_{560}) was normalized to $I_{R(570)}$ on a pixel-by-pixel basis, and $I_{F(560),baseline}$ was the baseline image at λ_{560} acquired immediately before electrical stimulation onset in each block. In this equation, negative values in $\Delta I_{F(560)}$ (i.e., a positive $-\Delta I_{F(560)}$) indicate increases in the SO_2 level and vice versa.²¹ The mean functional SO_2 changes [$R_{SO_2}(t)$] in a single vessel during the stimulation period were probed as follows:

$$\begin{aligned} R_{SO_2}(t) &= \frac{\sum_{(x,z) \in \text{vessel pixel}} [I_{F(560)}(x, z, t)]/A[I_{R(570)}(t)]}{\sum_{(x,z) \in \text{vessel pixel}} [I_{F(560),baseline}(x, z, t)]/A[I_{R(570),baseline}(t)]}. \end{aligned} \quad (4)$$

When $I_{R(570)}$ is used as a marker for HbT and $I_{F(560)}$ is used as a marker for SO_2 , the fPAM system can be used to probe the changes in HbT and SO_2 independently, as shown in Eqs. (2) and (4).

2.5 Statistical Analyses

The experiments were designed to quantitatively measure PA signal [$I_{R(570)}$] changes, as well as changes in the SSS and bilateral MI and MII arterioles, following electrical stimulation. Statistical significance was assessed using a paired t -test, with the significance defined as a probability (p) value of <0.05 . Side-to-side differences in PA signals [$I_{R(570)}$] and $\Delta I_{F(560)}$] of the studied areas and CBV changes were both examined using paired t -tests ($p < 0.05$, $n = 6$). The significance of changes observed in the fPAM signals [$\Delta I_{F(560)}$] of the studied areas in response to electrical stimulation was evaluated using the Wilcoxon matched-pairs signed-rank test (two-tailed, $p < 0.05$, $n = 6$). All statistical analyses were performed using SPSS (version 10.0, SPSS, IBM, Armonk, NY).

3 Results

3.1 HbT Changes in the Bilateral Cerebral Vessels During Stimulations of Different Intensities and Durations

The first rows of Fig. 3(a) and 3(b) show $R_{HbT}(t)$ in the SSS and bilateral MI and MII arterioles during 1 stimulation block and using the stimulation intensities of 1, 2, 6, and 10 mA, with a duration of 5 s. The yellow zone indicates the 5-s Stimulation-ON period. Significant HbT changes were observed in the SSS and MI and MII arterioles contralateral to the electrically stimulated left forepaw. In contrast, no significant HbT changes were found in the ipsilateral MI or MII arteriole. The time to peak R_{HbT} in the SSS and the contralateral MI and MII arterioles after stimulation onset using a stimulation intensity of 2 mA was 16.24, 9.68, and 19.75 s, respectively. There was no significant difference among the times to peak R_{HbT} in the SSS and contralateral MI and MII arterioles using any of these stimulation intensities. However, the peak R_{HbT} values were significantly higher than the baseline when these stimulation intensities were used. The average R_{HbT} response time was 26.56, 23.42, and 25.84 s for the SSS and the contralateral MI and MII arterioles, respectively. The response time is defined as the difference between the time of stimulation onset (i.e., 20 s in each stimulation block) and the time when the R_{HbT} value return to the baseline. Here the baseline is the R_{HbT} value obtained immediately before the stimulation onset. Note that the same definition is also applied to R_{CBV} and $-R_{SO_2}$.

Figure 4(a) shows the peak R_{HbT} values in the SSS and contralateral MI and MII arterioles as a function of stimulation intensity. Using a stimulation intensity of 2 mA, the peak R_{HbT} value was 0.98 ± 0.002 (mean \pm SD) ($p < 0.001$) in the SSS, 2.940 ± 0.003 (mean \pm SD) ($p < 0.001$) in the contralateral MI arteriole and 3.510 ± 0.004 (mean \pm SD) ($p < 0.001$) in the MII arteriole during stimulation (Wilcoxon matched-pairs signed-rank test, $n = 6$). Three additional statistically

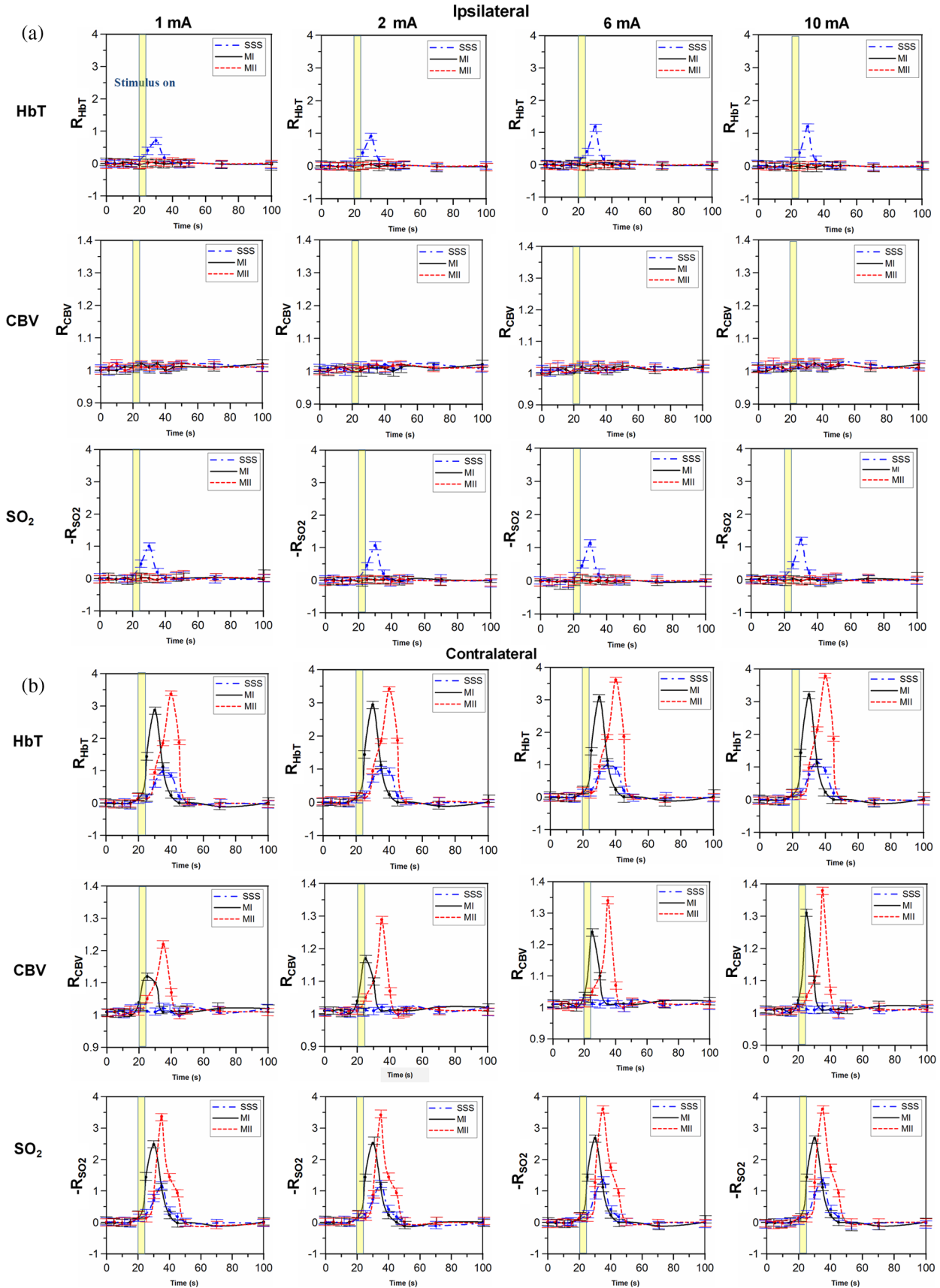


Fig. 3 Functional changes in the HbT, CBV, and SO_2 (i.e., R_{HbT} , R_{CBV} , $-R_{SO_2}$) in the SSS and bilateral MI and MII arterioles during one stimulation block, shown as a function of time under different stimulation intensities (1, 2, 6, and 10 mA) and with a duration of 5 s. (a) Ipsilateral. (b) Contralateral. The error bars represent the standard deviations of the data from six rats. The yellow zone indicates the 5-s Stimulation-ON period. Note that the ipsilateral SSS is the SSS during the ipsilateral-side measurement, and the contralateral SSS is the same SSS during the contralateral-side measurement.

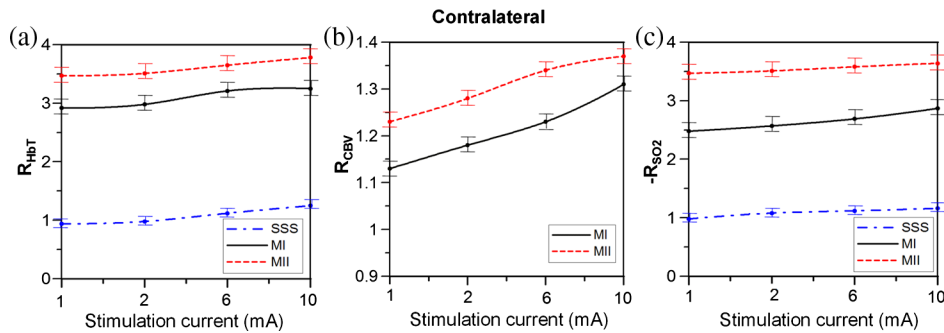


Fig. 4 Peak R_{HbT} , R_{CBV} , and $-R_{SO_2}$ values in the SSS and contralateral MI and MII arterioles during one stimulation block under a 5-s stimulation, plotted as a function of stimulation intensity. The error bars represent the standard deviations of the data from six rats. Note that the ipsilateral SSS is the SSS during the ipsilateral-side measurement, and the contralateral SSS is the same SSS during the contralateral-side measurement.

significant peak R_{HbT} values using stimulation intensities of 1, 6, and 10 mA are plotted in Fig. 4(a). There was a slight trend of increasing R_{HbT} peak amplitude with increasing stimulation intensity. No significant peak R_{HbT} values were observed in the ipsilateral MI or MII arterioles from Stimulation-ON to Stimulation-OFF ($p > 0.05$).

The first rows of Fig. 5 show $R_{HbT}(t)$ in the SSS and bilateral MI and MII arterioles in one 15-s stimulation block using a stimulation intensity of 2 mA. In this long stimulation, the time to peak R_{HbT} after stimulation onset in the SSS and the contralateral MI and MII arterioles was 18.41, 17.12, and 21.08 s, respectively. The times to peak R_{HbT} in the SSS and the contralateral MI and MII arterioles were longer than those using the 5-s stimulation. During stimulation, the peak R_{HbT} value using a 15-s stimulation was 1.16 ± 0.001 (mean \pm SD) ($p < 0.001$) in the SSS, 3.240 ± 0.003 (mean \pm SD) ($p < 0.001$) in the contralateral MI arteriole and 3.890 ± 0.004 (mean \pm SD) ($p < 0.001$) in the MII arteriole (Wilcoxon matched-pairs signed-rank test, $n = 6$). The peak R_{HbT} values were significantly higher when the 15-s stimulation was used than when the values from the 5-s stimulation were used.

Under the long stimulation condition, the response time of R_{HbT} from the R_{HbT} to baseline was 28.42, 23.75, and 26.14 s for the SSS and the contralateral MI and MII arterioles, respectively. Only the SSS and the contralateral MII showed longer response times when the 15-s stimulation was used. The response time of R_{HbT} in the contralateral MI vessel was only slightly increased compared with the shorter stimulation. The time to peak R_{HbT} of the contralateral MI arteriole increased significantly under the 15-s stimulation compared with 5 s; however, the times to peak R_{HbT} of the SSS and contralateral MII arteriole were not increased significantly.

3.2 CBV Changes in Bilateral Cerebral Vessels During Stimulations of Different Intensities and Durations

The second rows of Fig. 3(a) and 3(b) show $R_{CBV}(t)$ in the SSS and bilateral MI and MII arterioles in 1 stimulation block under stimulation intensities of 1, 2, 6, and 10 mA and a stimulation duration of 5 s. Using a stimulation intensity of 2 mA, the time to peak R_{CBV} was 8.34 s in the contralateral MI arteriole and 16.13 s in the contralateral MII arteriole after stimulation onset. There was no significant difference in the time to peak R_{CBV} between the contralateral MI and MII arterioles using any of the four stimulation intensities; however, the peak R_{CBV} values were significantly different between the MI and MII arterioles. The average R_{CBV} response time from the stimulation

onset to the return of R_{CBV} to baseline was 14.12 s in the contralateral MI arteriole and 20.78 s in the contralateral MII arteriole under a stimulation intensity of 2 mA [Fig. 3(b)].

Figure 4(b) shows the peak R_{CBV} values in the contralateral MI and MII arterioles as a function of stimulation intensity. Using a stimulation intensity of 2 mA, the peak R_{CBV} values in the contralateral MI and MII arterioles were 1.160 ± 0.003 (mean \pm SD) ($p < 0.0001$) and 1.270 ± 0.002 (mean \pm SD) ($p < 0.001$), respectively (paired t -test; $n = 6$). In contrast, neither the MI nor the MII arterioles displayed significant CBV changes ($p > 0.05$) in the hemispheres ipsilateral to the forepaw response region. Additionally, no significant R_{CBV} was found in the SSS during stimulation ($p > 0.05$). Another three significant peak R_{CBV} values using stimulation intensities of 1, 6, and 10 mA are plotted in Fig. 4(b). The results indicate that the peak R_{CBV} values were sensitive to the increasing stimulation intensities.

The second row of Fig. 5 shows $R_{CBV}(t)$ in the SSS and bilateral MI and MII arterioles in one stimulation block under 15-s stimulation. Using the long stimulation condition (Fig. 5), the R_{CBV} response times from the stimulation onset to the return of R_{CBV} to baseline were 17.85 and 22.38 s for the contralateral MI and MII arterioles, respectively.

3.3 SO_2 Changes in Bilateral Cerebral Vessels During Stimulations of Different Intensities and Durations

The third rows of Fig. 3(a) and 3(b) illustrate time course measurements of $-R_{SO_2}$ in the SSS and bilateral MI and MII arterioles in one stimulation block using stimulation intensities of 1, 2, 6, and 10 mA and a duration of 5 s. After stimulation onset at 2 mA, the time to peak $-R_{SO_2}$ was 12.14, 9.87, and 17.82 s in the SSS and contralateral MI and MII arterioles, respectively. There was no significant difference among the times to peak $-R_{SO_2}$ in the SSS and the contralateral MI and MII arterioles when any of the four stimulation intensities were being used. However, the peak $-R_{SO_2}$ values were significantly higher than baseline under these stimulation intensities. The peak $-R_{SO_2}$ values changed in proportion to the stimulation intensity. Using a 5-s stimulation, the average response times of $-R_{SO_2}$ from stimulation onset to the return of $-R_{SO_2}$ to baseline were 26.12, 22.87, and 24.96 s for the SSS and the contralateral MI and MII arterioles, respectively.

Figure 4(c) shows the peak $-R_{SO_2}$ values in the SSS and the contralateral MI and MII arterioles as a function of the stimulation intensity. The peak $-R_{SO_2}$ values during stimulation were 0.96 ± 0.002 (mean \pm SD) ($p < 0.001$) in the SSS, 2.490 ± 0.003 (mean \pm SD) ($p < 0.001$) in the contralateral

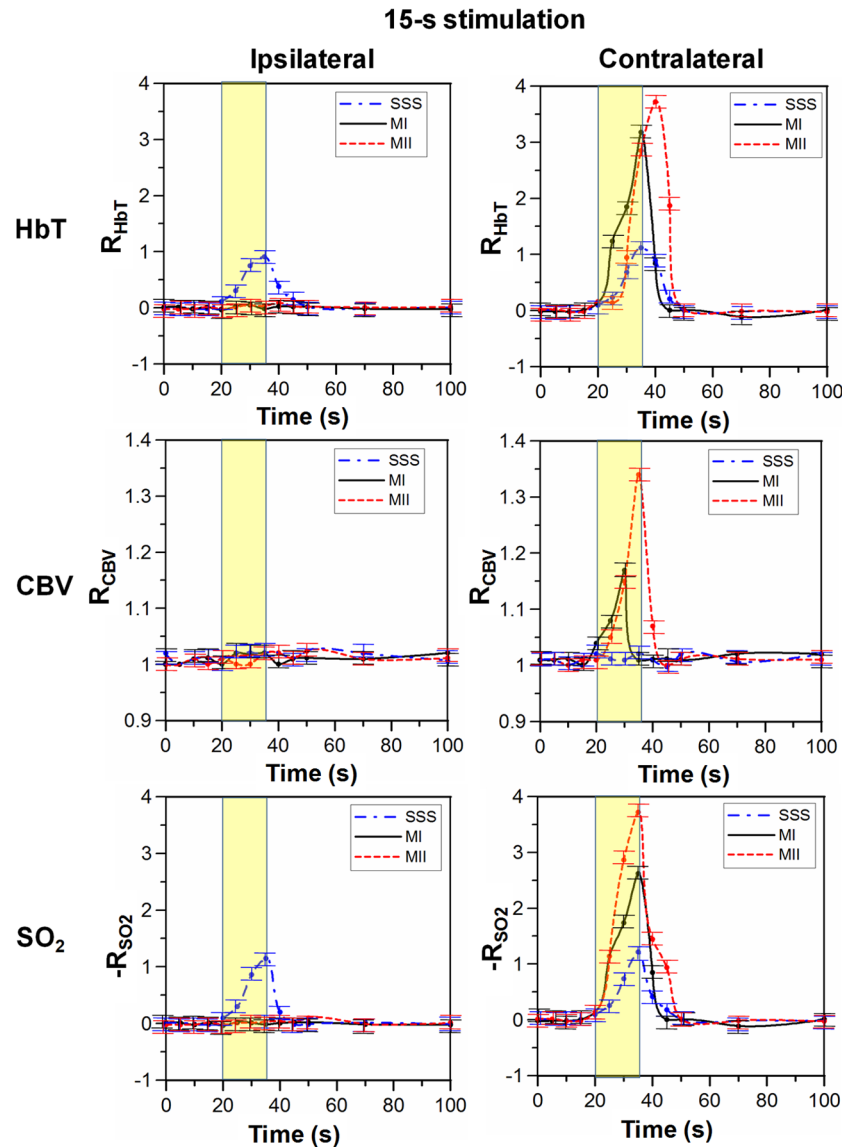


Fig. 5 Functional HbT, CBV, and SO_2 changes (i.e., R_{HbT} , R_{CBV} , $-R_{\text{SO}_2}$) in the SSS and bilateral MI and MII arterioles in one stimulation block as a function of time using 15-s stimulations of 2 mA. The error bars represent the standard deviations of the data from six rats. The yellow zone indicates the Stimulation-ON period. Note that the ipsilateral SSS is the SSS during the ipsilateral-side measurement, and the contralateral SSS is the same SSS during the contralateral-side measurement.

MI arteriole and 3.520 ± 0.004 (mean \pm SD) ($p < 0.001$) in the MII arteriole (Wilcoxon matched-pairs signed-rank test, $n = 6$) using a stimulation intensity of 2 mA. Slight peak $-R_{\text{SO}_2}$ increases accompanied the increasing stimulation intensities. No significant $-R_{\text{SO}_2}$ changes were observed in the ipsilateral MI or MII arterioles from Stimulation-ON to Stimulation-OFF ($p > 0.05$). Another three significant peak $-R_{\text{SO}_2}$ values using stimulation intensities of 1, 6, and 10 mA are plotted in Fig. 4(c). These results indicate that the peak $-R_{\text{SO}_2}$ values were sensitive to the increasing stimulation intensity.

The third row of Fig. 5 shows $-R_{\text{SO}_2}$ in the SSS and bilateral MI and MII arterioles in 1 15-s block using a 2-mA stimulation. For long stimulations, the time to peak $-R_{\text{SO}_2}$ in the SSS and the contralateral MI and MII arterioles was 15.51, 15.14, and 18.89 s, respectively, after stimulation onset. The peak $-R_{\text{SO}_2}$ values using the 15-s stimulation were 1.12 ± 0.001 (mean \pm SD) ($p < 0.001$) in the SSS, 3.140 ± 0.002 (mean \pm SD) ($p < 0.001$) in the contralateral MI arteriole, and

3.840 ± 0.005 (mean \pm SD) ($p < 0.001$) in the MII arteriole (Wilcoxon matched-pairs signed-rank test, $n = 6$). Using the long stimulation condition, the $-R_{\text{SO}_2}$ response times from stimulation onset to the return of $-R_{\text{SO}_2}$ to baseline were 27.62, 24.95, and 26.27 s in the SSS and the contralateral MI and MII arterioles, respectively. The time to peak $-R_{\text{SO}_2}$ in the contralateral MI arteriole was longer under the 15-s stimulation than the 5-s stimulation. However, the times to peak $-R_{\text{SO}_2}$ in the SSS and contralateral MII arterioles did not differ between the 15- and 5-s stimulations.

4 Discussion

The present study used fPAM to investigate the HRFs of the HbT, CBV, and SO_2 in the SSS and bilateral MI and MII arterioles in response to forepaw stimulations of various intensities and durations. Our main findings were as follows: (1) the HRFs of the HbT, CBV, and SO_2 in specific cerebral blood vessels can be investigated reliably using fPAM; (2) functional HbT

and SO_2 increased sublinearly (i.e., compressed) with increasing stimulation intensities; (3) the CBV changes, within a limited dynamic range of stimulation intensities and durations, were correlated more linearly than the HbT and SO_2 with the arterioles; (4) the times to peak HbT and CBV were lower in the MI arterioles than in the MII arterioles; and (5) the peak values of the HbT, CBV and SO_2 responses were higher in the MII arterioles than in the MI arterioles.

4.1 Functional Changes in the HbT, CBV, and SO_2 in Response to Various Stimulation Intensities

Our experiments in which various electrical stimulation intensities were applied to the left rat forepaw showed significant increases in contralateral HbT (i.e., increases in $I_{R(570)}$), CBV (i.e., increases in vascular cross-sectional area in $I_{R(570)}$) and SO_2 (i.e., negative $\Delta I_{F(560)}$ or decreases in $I_{F(560)}$) in the MI and MII arterioles. In the SSS, significant increases in HbT and SO_2 were observed under various stimulation intensities (1, 2, 6, and 10 mA) of fixed duration (5 s), whereas the CBV in the SSS did not increase under any stimulation. With increasing stimulation intensities, the maximum functional HRF changes in the HbT and SO_2 were sub-linear (i.e., compressed) phenomena.¹⁰ The peak values of the CBV were more linearly correlated with increasing stimulation intensities in arterioles than the peak HbT and SO_2 . This result implies that saturation in neural activation occurs at a stimulation intensity larger than 2 mA. According to a previous study,³⁴ a similar phenomenon has been found in response to an amplitude of about 1.5 mA. On the other hand, our results suggest that the larger CBV changes were more significantly correlated to the local activation region. An explanation for this is that with increasing stimulation intensity, the local activation region demands more oxygenated blood, while more deoxygenated blood drains out of the activation region, resulting in the CBV changing significantly and linearly with the stimulation intensity, especially in the arterioles.^{2,3} The oxygenated and deoxygenated blood will afflux into the smaller arterioles and induce more significant CBV changes than the changes in HbT and SO_2 . Nemoto et al. also showed that the CBV-related signals are more highly correlated than oxygenation-related signals with the activated region.³⁵

In addition, the phenomena of HbT and SO_2 onset overshoots may be due to blood flow increases near the local activation sites, which would lead to a fresh blood supply and greater HbT and SO_2 increases in the surrounding arterioles.¹⁵ The oxygenated blood that subsequently flows into the veins may lead to HbT and SO_2 increases.^{2,36} The current fPAM system found that the times to peak HbT and SO_2 were shorter in the MI arterioles than in veins under different stimulation intensities. To transfer a significant amount of HbT and SO_2 into the activation region, shorter times are needed to reach peak HbT and SO_2 in MI arterioles than in veins.^{15,36,37} Moreover, the greater increases in the HbT and SO_2 levels also indicate increased CBF.³² This finding of dissociation of the HbT and CBV responses strongly suggests that Grubb's relationship between CBF and CBV [$\text{CBV} = 0.8 \times \text{CBF}$ (Ref. 38)] does not always apply and requires revision.² Additionally, a significant lateralization phenomenon during different unilateral forepaw electrical stimulation intensities was observed, in agreement with previous studies.^{15,39,40}

With changing stimulation intensities, HRF changes in HbT, CBV, and SO_2 were all faster in the contralateral MI arteriole than in the contralateral MII arteriole. This occurred because the HRF results in these increases in large blood vessels before

smaller blood vessels.⁴¹ Conversely, the peak values of HbT, CBV, and SO_2 were larger in the contralateral MII arteriole than in the contralateral MI arteriole. A potential explanation for this is that the contralateral MII arteriole is closer to the activated cerebral regions than the contralateral MI arteriole.^{2,42} To transfer a significant quantity of oxygenated blood into the activated region during the stimulation period, the peak changes in HbT, CBV, and SO_2 in the contralateral MII arteriole must be larger than those in the contralateral MI arteriole.⁴² These results indicate that the HRF is affected by the stimulation intensity.²

4.2 Functional HbT, CBV, and SO_2 Changes in Response to Various Stimulation Durations

Our findings suggest that the response times of CBV, HbT, and SO_2 in single blood vessels are independent of the stimulation duration. Therefore, the response times of CBV, HbT, and SO_2 in those blood vessels will not be affected significantly by stimulation duration. Rather, only the degrees of CBV, HbT, and SO_2 changes are affected by stimulation duration.^{2,3} DOI can measure hemodynamic changes from only a selected region of interest,^{9,10} but not the changes in single vessels, as presented in this study. This fact may explain the previously reported plateau response phenomenon after stimulation onset, as well as the longer response time compared to the shorter stimulation duration when measuring changes in HbT, CBV, and SO_2 .^{3,10} We were only interested in the HRF changes in single blood vessels, not the total changes from the selected region of interests. The same problems also exist when using fMRI, which senses only the changes in response to stimulation from selected pixels, not a single cerebral vessel. Thus, the stimulation-induced HRF changes in single vessels cannot be measured directly by fMRI.⁴

In addition, the results under different stimulation durations (5 and 15 s) indicate that relative functional HbT, CBV, and SO_2 changes were more strongly correlated in the contralateral MI arteriole than in the contralateral MII arteriole. It is possible that the contralateral MII arteriole is closer to the activation region and that its cross-section is also smaller than that of the contralateral MI arteriole, which would lead the MII arterioles to reach their maximum blood volume soon after stimulation onset.² Therefore, using longer stimulation, smaller functional hemodynamic changes in the contralateral MII arteriole were found. However, our data suggest that changes in HbT, CBV, and SO_2 are more prominently associated with smaller arterioles using stimulations of different intensities and durations.² This finding, consistent with fMRI data of previous studies,⁴² can be attributed to the immediate proximity of the neuronal activity to the smaller arterioles.

Our data also suggest that HbT, CBV, and SO_2 responses remained elevated for a few seconds after the onset of the stimulation in the contralateral MI and MII arterioles under different stimulation intensities (1, 2, 6, and 10 mA) and durations (5 and 15 s). In delivering blood flow and oxygenation to locally activated tissues, the total response times of HbT, CBV, and SO_2 are longer in smaller arteries than in large ones,^{2,43} likely due to the locations of the smaller arteries.

In addition, our findings demonstrate that HbT changes in the SSS were significant, but there were no significant CBV changes. This finding appears contradictory because HbT and CBV, despite being calculated using different techniques, should be relatively similar. There are two potential reasons for this discrepancy: (1) because the SSS is the largest vein in the rat brain, small changes in its cross-section are difficult to detect, whereas

changes in CBV could cause large changes in HbT; and (2) the CBV calculation requires an accurate image of a specific blood vessel to calculate the cross-sectional area. Although the SSS could be seen in the PA B-scan images, the PA signals from the SSS were much weaker than those from other cortical vessels.^{21,27} This difficulty may have resulted from the spherical geometric focusing and the finite detection bandwidth of the 50-MHz ultrasound transducer that was used in our current fPAM setup. Concordant with our results, a previous study has indicated significant SO₂ changes in veins and arterioles, with significant CBV changes seen only in arterioles during somatosensory stimulation.⁴³

5 Conclusions

The present study demonstrates the unique capabilities of an fPAM system for characterizing the HRF changes in single cerebral blood vessels. Local relative functional HRFs (i.e., HbT, CBV, and SO₂) in single blood vessels using different stimulation intensities (1, 2, 6, and 10 mA) and durations (5 and 15 s) were analyzed and discussed comprehensively. Our results indicate that both the times to reach the peak values and the magnitudes of the peak values of the HbT, CBV, and SO₂ responses were faster and higher, respectively, in the MII arterioles than in the MI arterioles. This may have occurred because the MII arterioles, which are smaller, are much closer to the local activated region and, therefore, require greater metabolism. We also found that integrated CBV increased more linearly with stimulation intensity and duration than did the HbT or SO₂, which indicates that the significant CBV changes were more colocalized with the neuronal activation and corresponding blood consumption. Our findings are concordant with those reported in the literature, indicating that the regulation of hemodynamic changes in single blood vessels can be studied reliably by fPAM without the use of contrast agents. The current fPAM system will be useful as a complementary modality to other neurovascular imaging techniques for label-free investigations of HRFs to assess neuronal activity in single cerebral blood vessels.

Acknowledgments

We acknowledge the National Science Council, R.O.C., for its support of this research (NSC Nos. 97-2221-E-007-084-MY3, NSC 100-2221-E-007-010-MY2, 96-2220-E-009-029, 97-2220-E-009-029, 99-2221-E-009-154, and 99-2911-I-009-101), as well as funding support from the National Tsing Hua University (Boost program 98N2531E1) and the Ministry of Education, Taiwan. The authors would also like to thank Po-Hsun Wang for his help in developing the fPAM system.

References

1. R. Buxton, "Interpreting oxygenation-based neuroimaging signals: the importance and the challenge of understanding brain oxygen metabolism," *Front. Neuroenerg.* **2**(8), 1–16 (2010).
2. A. Seiyama et al., "Regulation of oxygen transport during brain activation: stimulus-induced hemodynamic responses in human and animal cortices," *Dyn. Med.* **2**(1), 6–16 (2003).
3. Y. Hirano, B. Stefanovic, and A. C. Silva, "Spatiotemporal evolution of the functional magnetic resonance imaging response to ultrashort stimuli," *J. Neuro.* **31**, 1440–1447 (2011).
4. C.-Y. Lin et al., "In vivo cerebromicrovasculature visualization using 3D [Delta]R2-based microscopy of magnetic resonance angiography (3D[Delta]R2-mMRA)," *NeuroImage* **45**, 824–831 (2009).

5. E. M. C. Hillman, "Optical brain imaging in vivo: techniques and applications from animal to man," *J. Biomed. Opt.* **12**(5), 051402 (2007).
6. D. Malonek and A. Grinvald, "Interactions between electrical activity and cortical microcirculation revealed by imaging spectroscopy: implications for functional brain mapping," *Science* **272**, 551–554 (1996).
7. S. Prahl, *Optical Spectra*, <http://omlc.ogi.edu/> (2007).
8. L. V. Wang and H.-i. Wu, *Biomedical Optics: Principles and Imaging* Wiley, New York (2007).
9. J. P. Culver et al., "Evidence that cerebral blood volume can provide brain activation maps with better spatial resolution than deoxygenated hemoglobin," *NeuroImage* **27**, 947–959 (2005).
10. A. M. Siegel et al., "Temporal comparison of functional brain imaging with diffuse optical tomography and fMRI during rat forepaw stimulation," *Phys. Med. Biol.* **48**, 1391–1403 (2003).
11. M. Peng et al., "High resolution cerebral blood flow imaging by registered laser speckle contrast analysis," *IEEE Trans. Biomed. Eng.* **57**, 1152–1157 (2010).
12. N. Li et al., "High spatiotemporal resolution imaging of the neurovascular response to electrical stimulation of rat peripheral trigeminal nerve as revealed by in vivo temporal laser speckle contrast," *J. Neurosci. Meth.* **176**, 230–236 (2009).
13. H. Dehghani et al., "Numerical modelling and image reconstruction in diffuse optical tomography," *Philos. Trans. Royal Soc. A: Math. Phys. Eng. Sci.* **367**, 3073–3093 (2009).
14. G. Gratton and M. Fabiani, "Dynamic brain imaging: event-related optical signals (EROS) measures of the time course and localization of cognitive-related activity," *Psychonomic Bull. Rev.* **5**, 535–563 (1998).
15. M. B. Bouchard et al., "Ultra-fast multispectral optical imaging of cortical oxygenation, blood flow, and intracellular calcium dynamics," *Opt. Express* **17**, 15670–15678 (2009).
16. P. Miao et al., "Random process estimator for laser speckle imaging of cerebral blood flow," *Opt. Express* **18**, 218–236 (2010).
17. H. F. Zhang, K. Maslov, and L. V. Wang, "In vivo imaging of subcutaneous structures using functional photoacoustic microscopy," *Nat. Protocols* **2**, 797–804 (2007).
18. S. A. Ermilov et al., "Laser photoacoustic imaging system for detection of breast cancer," *J. Biomed. Opt.* **14**(2), 024007 (2009).
19. H. F. Zhang et al., "Functional photoacoustic microscopy for high-resolution and noninvasive in vivo imaging," *Nat. Biotech.* **24**, 848–851 (2006).
20. L. V. Wang, "Multiscale photoacoustic microscopy and computed tomography," *Nat. Photon.* **3**, 503–509 (2009).
21. L.-D. Liao et al., "Imaging brain hemodynamic changes during rat forepaw electrical stimulation using functional photoacoustic microscopy," *NeuroImage* **52**, 562–570 (2010).
22. G. Paxinos and C. Watson, *The Rat Brain in Stereotaxic Coordinates*, Academic Press, San Diego (2007).
23. Y.-Y. Chen et al., "MicroPET imaging of noxious thermal stimuli in the conscious rat brain," *Somatosens. Motor Res.* **27**, 69–81 (2010).
24. B. P. Chugh et al., "Measurement of cerebral blood volume in mouse brain regions using micro-computed tomography," *NeuroImage* **47**, 1312–1318 (2009).
25. G. Paxinos, *The Rat Nervous System*, 3d ed. Elsevier Academic Press, San Diego (2004).
26. R. Weber et al., "Early prediction of functional recovery after experimental stroke: functional magnetic resonance imaging, electrophysiology, and behavioral testing in rats," *J. Neuro.* **28**, 1022–1029 (2008).
27. E. W. Stein, K. Maslov, and L. V. Wang, "Noninvasive, in vivo imaging of blood-oxygenation dynamics within the mouse brain using photoacoustic microscopy," *J. Biomed. Opt.* **14**(2), 020502 (2009).
28. M.-L. Li et al., "Improved in vivo photoacoustic microscopy based on a virtual-detector concept," *Opt. Lett.* **31**, 474–476 (2006).
29. J. B. Mandeville et al., "MRI measurement of the temporal evolution of relative CMRO₂ during rat forepaw stimulation," *Mag. Res. Med.* **42**, 944–951 (1999).
30. A. C. Silva et al., "Simultaneous blood oxygenation level-dependent and cerebral blood flow functional magnetic resonance imaging during forepaw stimulation in the rat," *J. Cere. Blood Flow Metab.* **19**, 871–879 (1999).
31. K. J. Friston et al., "Event-related fMRI: characterizing differential responses," *NeuroImage* **7**, 30–40 (1998).

32. S. Roston, "The blood flow of the brain," *Bull. Math. Biol.* **29**, 541–548 (1967).
33. L. Li et al., "Photoacoustic imaging of lacZ gene expression in vivo," *J. Biomed. Opt.* **12**(2), 020504 (2007).
34. C. Spenger et al., "Functional MRI at 4.7 Tesla of the rat brain during electric stimulation of forepaw, hindpaw, or tail in single- and multislice experiments," *Exper. Neur.* **166**, 246–253 (2000).
35. M. Nemoto et al., "Functional signal- and paradigm-dependent linear relationships between synaptic activity and hemodynamic responses in rat somatosensory cortex," *J. Neur.* **24**, 3850–3861 (2004).
36. I. Y. Petrova et al., "Noninvasive monitoring of cerebral blood oxygenation in ovine superior sagittal sinus with novel multi-wavelength photoacoustic system," *Opt. Express* **17**, 7285–7294 (2009).
37. E. Vovenko, "Distribution of oxygen tension on the surface of arterioles, capillaries and venules of brain cortex and in tissue in normoxia: an experimental study on rats," *Pflügers Archiv Eur. Phys. J.* **437**, 617–623 (1999).
38. R. L. J. Grubb et al., "The effects of changes in PaCO₂ cerebral blood volume, blood flow, and vascular mean transit time," *Stroke* **5**, 630–639 (1974).
39. G. McCarthy et al., "Functional magnetic resonance imaging of human prefrontal cortex activation during a spatial working memory task," *Proc. Natl. Acad. Sci. USA* **91**, 8690–8694 (1994).
40. Y.-Y. I. Shih et al., "A new scenario for negative functional magnetic resonance imaging signals: endogenous neurotransmission," *J. Neuro.* **29**, 3036–3044 (2009).
41. M. E. Raichle and H. L. Stone, "Cerebral blood flow autoregulation and graded hypercapnia," *Eur. Neurol.* **6**, 1–5 (1971).
42. T. B. Harshbarger and A. W. Song, "Endogenous functional CBV contrast revealed by diffusion weighting," *NMR in Biomed.* **19**, 1020–1027 (2006).
43. E. M. C. Hillman et al., "Depth-resolved optical imaging and microscopy of vascular compartment dynamics during somatosensory stimulation," *NeuroImage* **35**, 89–104 (2007).